



Removal of ciprofloxacin from water through magnetic nanocomposite/membrane hybrid processes

Azmat Ullah, Muhammad Zahoor*, Sultan Alam

Department of Chemistry, University of Malakand, Chakdara, Dir Lower, 18800 KPK, Pakistan,

emails: mohammadzahoorus@yahoo.com (M. Zahoor), azmatullah9499@gmail.com (A. Ullah), dr.sultanalam@yahoo.com (S. Alam)

Received 3 April 2018; Accepted 22 September 2018

ABSTRACT

In this study a novel adsorbent, magnetic carbon nanocomposites (MCNs), was prepared from biomass precursors of pineapple and was characterized by SEM (scanning electron microscopy), XRD (X-ray diffraction), FTIR (Fourier transform infrared), thermal gravimetric/differential thermal analysis, energy dispersive X-ray, surface area analyzer, and $\text{pH}_{\text{(pzc)}}$. The presence of iron oxide on the adsorbent surface was confirmed from SEM, XRD, and FTIR analysis. The adsorbent was then used for the removal ciprofloxacin (CIP) from water by batch adsorption and adsorption/membrane hybrid processes. Freundlich, Langmuir, and Temkin isotherms were used for the determination of adsorption parameters. The effects of pH, temperature, time, concentration, adsorbent dosage, humic acid, and ionic strength on adsorption process were evaluated. The adsorbent after use was regenerated using NaOH, methanol, and distilled water. The equilibrium time at pH 7 was 80 min. The kinetics data were applied to both first-, second-order pseudo kinetics, and intraparticle diffusion models. Pseudo-second-order kinetics was found best model that fits well the kinetics adsorption data. The values of ΔH° and ΔS° were -20 and 82 kJ/mol respectively. The values of ΔG° were negative: -23.672 , -25.666 , and -27.286 kJ/mol correspondingly to 25°C , 40°C , and 60°C . Improved permeate fluxes and percent retentions of CIP by membranes were observed for adsorption/membrane hybrid process MCN/UF (magnetic carbon nanocomposite/ultrafiltration), MCN/NF (magnetic carbon nanocomposite/nanofiltration), and MCN/RO (magnetic carbon nanocomposite/reverse osmosis filtration). The percent retention of CIP molecules in NF was 96% which increased to 100% when membrane was used in hybrid manner with MCN.

Keywords: Magnetic carbon nanocomposites; Iron oxide; Ultrafiltration membrane; Nanofiltration membrane; Reverse osmosis membrane

1. Introduction

In recent years, the occurrence of antibiotics in the environment has been recognized as an emerging environmental issue. Although they are important in prevention and treatment of infectious diseases, about 50%–90% of antibiotics administered to humans or animals are excreted via urine and feces as a mixture of parent drug and their metabolites into environment. These antibiotics in the aquatic environment causes drug resistance problems [1–3]. Fluoroquinolones such as ciprofloxacin and levofloxacin are

a third generation group of antibiotics. They are widely used in the treatment of infectious diseases in humans as well as animals. The presence of fluoroquinolones in the environment causes severe threats to human beings and antibiotics resistance in bacteria making the use of current antibiotics ineffective in the treatment of curable diseases such as cholera and typhoid [4–6].

Membrane processes due to their easy handling and speedy nature of the processes have replaced the conventional methods [7,8]. A number of membranes like microfiltration, ultrafiltration (UF), nanofiltration (NF), and reverse osmosis (RO) membranes are frequently used for this purpose. These membranes have pores of molecular dimension

* Corresponding author.

and thus have different molecular weight cut offs (MWCO), the presence of natural and synthetic pollutants affects the efficiencies of these membranes [9,10]. The pollutants present in water are stopped by membrane which accumulate near its surface, then some of which is adsorbed on the membrane surface resulting in blockage of the pores of membranes and thus adversely affect the permeate flux. So to remove this drawback activated carbon was used in hybrid manner with membrane processes [11–13], initially it was considered that activated carbon would adsorb the pollutants and if its particles enter into membrane system would form a porous layer on membrane surface and will not affect the permeate flux of the membrane, however, later on, it was found that the porous cake formed also affected the permeate flux. To remove this drawback, the activated carbon was made magnetic by Zahoor et al. [14–16], used magnetic activated carbon as an alternative for activated carbon in the membrane hybrid processes [11–13]. Magnetic activated carbon on one hand has magnetic character due to which it can be removed after use from slurry through application of a magnet and on the other hand it has comparable surface area [14–19].

This study was aimed to prepare magnetic carbon nano-composite (MCN) from biomass, characterized it through various instrumental techniques and to determine its potential for the removal of CIP from water through adsorption and adsorption/membrane processes in a hybrid manner. The adsorbent was used in a hybrid manner with UF, NF, and RO membranes.

2. Experimental

2.1. Chemicals

All the chemicals used in this study were of analytical grade and were purchased from Sigma-Aldrich, Germany. CIP antibiotic was collected from Swat Pharma, District Swat (Pakistan). The characteristic properties of CIP are given in Table 1. Double distilled water was used throughout the experimental work.

2.2. Preparation of MCN

A novel method was devised for the preparation of MCN from biomass. The dried biomass precursors of pineapple were cut into small pieces and transferred into a container containing the suspension of ferric chloride and ferrous

sulfate and 5 mol/L (100 mL) NaOH was added dropwise to the mixture at 70°C with constant stirring. The treated biomass was then dried in oven which was then charred and ignited for 10 h in an atmosphere of N₂ gas in a specially designed chamber containing an electric heater and wire gauze with an inlet for N₂ gas and an exhaust for various gases. The final product was washed with 1 mol/L HCl solution and washed with distilled water several times to attain the neutral pH 7. The final product was dried at 70°C in an electric oven.

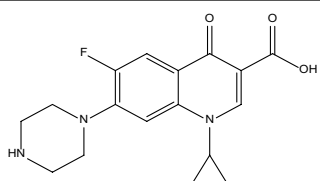
2.3. Characterization of MCN

MCN was characterized by X-ray diffraction (XRD) (with Nickel filter using monochromatic Cu K α rays, having wave length of 1.5418 Å). The X-ray generator was operated at current of 30 mA and voltage 40 KV. The scanning speed and scanning range were 10 min⁻¹ and 2 θ / θ , respectively. Fourier transform infrared (FTIR) spectrophotometer, Shimadzu, Japan was used in range from 450 to 4,000 cm⁻¹ to determine the surface functional groups of adsorbent. The surface morphology of MCN was determined using scanning electron microscopy (SEM) at accelerating voltage of 20 KV. The energy dispersive X-ray (EDX) analysis was done through EDS X-sight apparatus. The thermal gravimetric analysis (TGA) and differential thermal analysis (DTA) was performed with diamond series TGA/DTA Perkin Elmer, US analyzer using alumina (Al₂O₃) as a reference. The surface area of the MCN was measured with surface area analyzer (Quantachrome NovaWin instrument version-11.04) Nova station B, whereas point of zero charge was determined using mass titration method. For the determination of pH_(pzc) mass titration method was used. In this method various amounts of MCN were added to distilled water and resulting pH values were measured after 24 h of equilibration. Typical values of MCN/distilled water by weight were 0.01%, 0.05%, 0.1%, 0.2%, 0.3%, 0.4%, and 0.5%. Distilled water has been used after treatments of heating and cooling, and bubbling nitrogen under a nitrogen atmosphere. The containers of MCN/water were sealed and placed on a shaker for 24 h. All the experiments were conducted under nitrogen atmosphere.

2.4. CIP adsorption

The general methodology used in this study was to allow a specified amount of MCN in 100 mL flasks, each containing 50 mL CIP solution having the desired concentration according to the requirement of our experiment. In order to correct for any sorption of CIP due to container walls, control experiments were conducted without MCN, and there was negligible adsorption by the container walls. All the experiments were carried out in triplicate. The mean values were determined and presented in the form of plots and tables. The flasks were placed in a rotary shaker and were shaken at a speed of 150 rpm for a specified interval of time. The temperature was adjusted to the desired value (298 K). The solution pH was adjusted using 0.1 mol/L HCl and 0.1 mol/L NaOH solutions. The MCN was removed from solution through a magnetic bar. The CIP solution in the flasks was then filtered through Whatman filter paper N0. 1. The supernatants were checked for CIP concentration using UV/Visible

Table 1
Characteristic properties of the CIP used in this study

Structural formula of ciprofloxacin	
Molar mass	331.346 g/mol
Appearance	White crystalline
Dissociation constant	6.09–8.74 (at 298 K)
Solubility	Water soluble

spectrophotometer at 275 nm. The amount of CIP adsorbed q_e (mg/g) was calculated using the following relation:

$$q_e = (C_o - C_e) \times \frac{V}{W} \quad (1)$$

where C_o is initial CIP concentration in mg/dm³, C_e is the CIP concentration in mg/dm³ after certain interval of time, q_e is the amount of CIP adsorbed on the surface of MCN in mg/g, V is the volume of CIP solution in dm³, and W is the amount of MCN in grams. The percent removal rate (%R) was calculated using the following relation:

$$\% \text{ Removal rate} = \left(\frac{C_o - C_e}{C_o} \right) \times 100 \quad (2)$$

2.4.1. Adsorption kinetics

For the adsorption kinetics studies, 0.04 g of MCN was added to a series of 50 mL flasks containing 40 and 80 mg/L CIP solutions. The flasks were shaken from 0 to 240 min at 150 rpm at 298 K. Pseudo-first-order kinetics, pseudo-second-order kinetics, and intraparticle diffusion models were used to analyze the adsorption kinetic data.

2.4.2. Adsorption isotherm studies

50 mL of CIP solutions of different concentration, that is, 20–120 mg/L were taken in a series of flasks each containing 0.04 g of MCN. The flasks were shaken at 298 K for 80 min. The MCN was removed from solution using a magnetic bar. The CIP solution in flasks was then filtered through Whatman No. 1 filter paper and the supernatants were checked for CIP concentration using UV/visible spectrophotometer at 275 nm. Langmuir, Freundlich, and Temkin isotherm model equations were applied to the adsorption isotherm experimental data.

2.5. Determination of thermodynamic parameters

About 0.04 g of MCN was added to 50 mL (70 mg/L) CIP solution in 100 mL flasks. All the flasks were placed on shaker with a speed of 150 rpm at 25°C, 40°C, and 60°C each for 80 min. The MCN was then separated from the solution using magnetic bar. The solution was then filtered through Whatman filter paper No. 1 and analyzed for CIP concentration by UV-Visible spectrophotometer as discussed earlier.

2.6. Effect of the adsorbent dose and pH on CIP removal

The effect of adsorbent dosage, that is, from 0.01 to 0.06 g at initial CIP concentration of 30 mg/L was determined at 298 K.

The effect of pH, that is, from 3 to 11 at initial CIP concentration of 40 mg/L was determined at 298 K. The solution pH was adjusted using 0.1 M NaOH and 0.1 M HCl solutions.

2.7. Effect of humic acid

The effect of humic acid (HA) was determined using a different concentration of HA, that is, from 0 to 80 mg/L in

combination with CIP solution using 0.04 g MCN at 298 K for 240 min of shaking.

2.8. Effect of ionic strength on adsorption capacity of MCN

The effect of ionic strength was determined using different concentrations of NaCl (0–0.2 M) in combination with 30 mg/L CIP solution using 0.04 g MCN at 298 K for 240 min time of shaking.

2.9. Removal of CIP by membrane process

Three membranes UF, NF, and RO were used in this study in order to determine the % retention of selected antibiotic by each membrane and their consequent effect on permeate flux. The characteristic properties of these membranes are given in Tables 2–4. Membranes were first washed with distilled water as instructed by the manufacturer. A solution of known concentration of CIP was prepared in distilled water. All samples were equilibrated to room temperature, at pH 7 and applied transmembrane pressure was 1.0 bar throughout the experimental cycle. The rejection of CIP and the decline in the flow rate by the membrane alone were determined.

2.10. Membrane hybrid process

An attempt was made to compensate the resulting decline in permeate flux due to blockage of membrane pore by antibiotic through naked membrane. For this purpose MCN was used for the adsorption of CIP which reduces the CIP concentration in the feed water to the membrane system. A specially designed pilot plant was used for this purpose (Fig. 1). The membranes were washed with distilled water and water permeate flux was noted. The test solutions were taken in 12 L container and passed through UF/NF/RO membranes using the multispeed water pump. The membranes were then used in combination with the continuous stirred reactor, where MCN was added to the CIP solution in a single dose and was stirred for 1 h before feeding to the membranes system.

Table 2
Characteristic properties of UF membrane

Parameters	Specification
Material	Polyether sulfone
Type	Capillary multi bores × 7
Diameter bores ID	0.9 mm
Diameter fiber OD	4.2 mm
MWCO	100 KD
Surface area	50 m ²
Maximum temperature	40°C
Maximum pressure	7.5 bar
Membrane back wash pressure	0.5–1 bar
Operator pH range	3–10
Back wash pH range	1–13
Disinfection chemicals	
Hypochloride (NaOCl)	50–200 mg/L
Hydrogen peroxide (H ₂ O ₂)	100–200 mg/L

The UF membrane system was operated in dead-end mode. A specially designed container equipped with the magnetic arrangement was put in the assembly for the separation of MCN through magnet after use.

The membrane parameter like percent retention of CIP and their effect on permeate flux were determined. The percent retention of the solute R was determined by using the following relation:

$$R = \left(1 - \frac{C_p}{C_b} \right) \times 100 \quad (3)$$

where C_p is the concentration of solute in permeate (after passing through membrane) and C_b is the solute concentration in bulk (before feeding to membrane).

The permeate flux of membranes (J) L/m²/h was calculated at different time of filtration using the following relation:

$$J = \frac{1}{A} \cdot \frac{dv}{dt} \quad (4)$$

where A is area of membrane (m²), V is permeate volume (L), and t is filtration time (h).

Backwashing of each membrane was applied after each successive experimental cycle.

Table 3
Characteristics properties of NF membrane (DOW Film Tec 2.5 × 40)

Parameters	Specification
Model	NF 270-2540
Permeate Flow rate	850 gal/d (3.2 m ³ /d)
Active surface area	28 ft ² (3.2 m ²)
Applied pressure	4.8 bar
Stabilized salt rejection	>97%

Table 4
Characteristic properties of RO membrane (DOW FILMTEC ECO PRO 400i)

Parameters	Specification
Model	RO 270-2540
Membrane type	Thin film composite (Filmtech)
Permeate flow rate	850 gal/d (3.2 m ³ /d)
Active surface area	28 ft ² (3.2 m ²)
Maximum operating pressure	1.0 bar
Stabilized salt rejection	99.5%
pH range continuous operation	3–10
pH range short term cleaning	1–12

2.11. Regeneration and recycling of MCN (desorption experiment)

To evaluate the regeneration and recyclization of MCN desorption experiments were carried out. For this purpose, 0.15 g of MCN was added to 50 mL of 80 mg/L CIP solution at 298 K and pH 7.0. The reaction mixture was oscillated at 150 rpm for 6 h. The MCN/CIP complex was isolated from the reaction mixture using a magnet. The MCN/CIP solid was washed with 3% NaOH solution, methanol, and distilled water. The above-mentioned process was repeated five times until the CIP concentration was lower than 0.04 mg/L. At last MCN was oven dried at 70°C for 150 min. The recycling test was conducted six times.

3. Results and discussions

3.1. Characterization of the adsorbents

The nanocomposite was prepared on the carbon surface. The magnetic property of MCN was checked with a magnetic bar, after synthesis. The prepared nanocomposite completely adhered to magnetic bar confirming the magnetic character of the prepared MCN.

The EDX of MCN is shown in Fig. 2(a). The figure shows the presence of carbon (C), iron (Fe), oxygen (O), etc.

Figs. 2(b)–(d) show SEM images of MCN. SEM gives us valuable information about the morphology of MCN. SEM images show that prepared MCN is having an average size of 45–65 nm. The particle size of MCN is narrowly distributed.

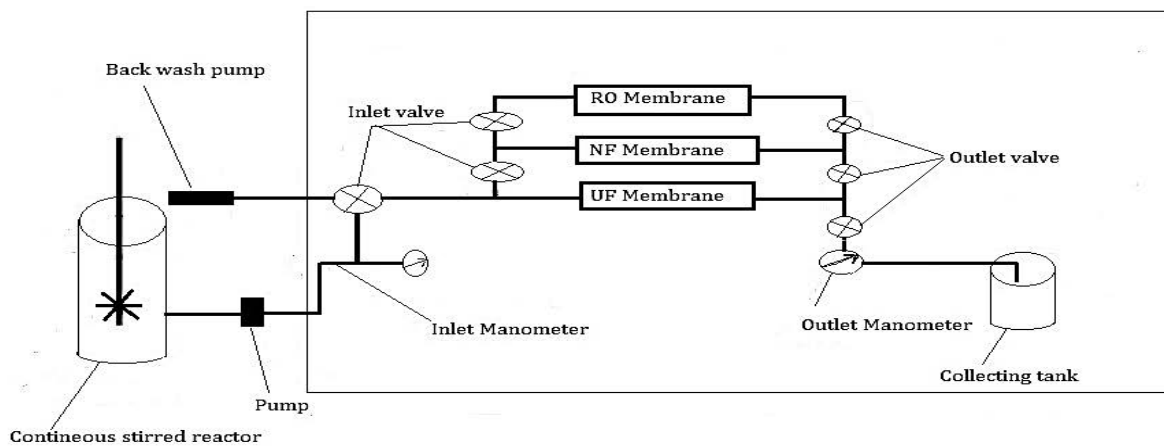


Fig. 1. Membrane hybrid pilot plant.

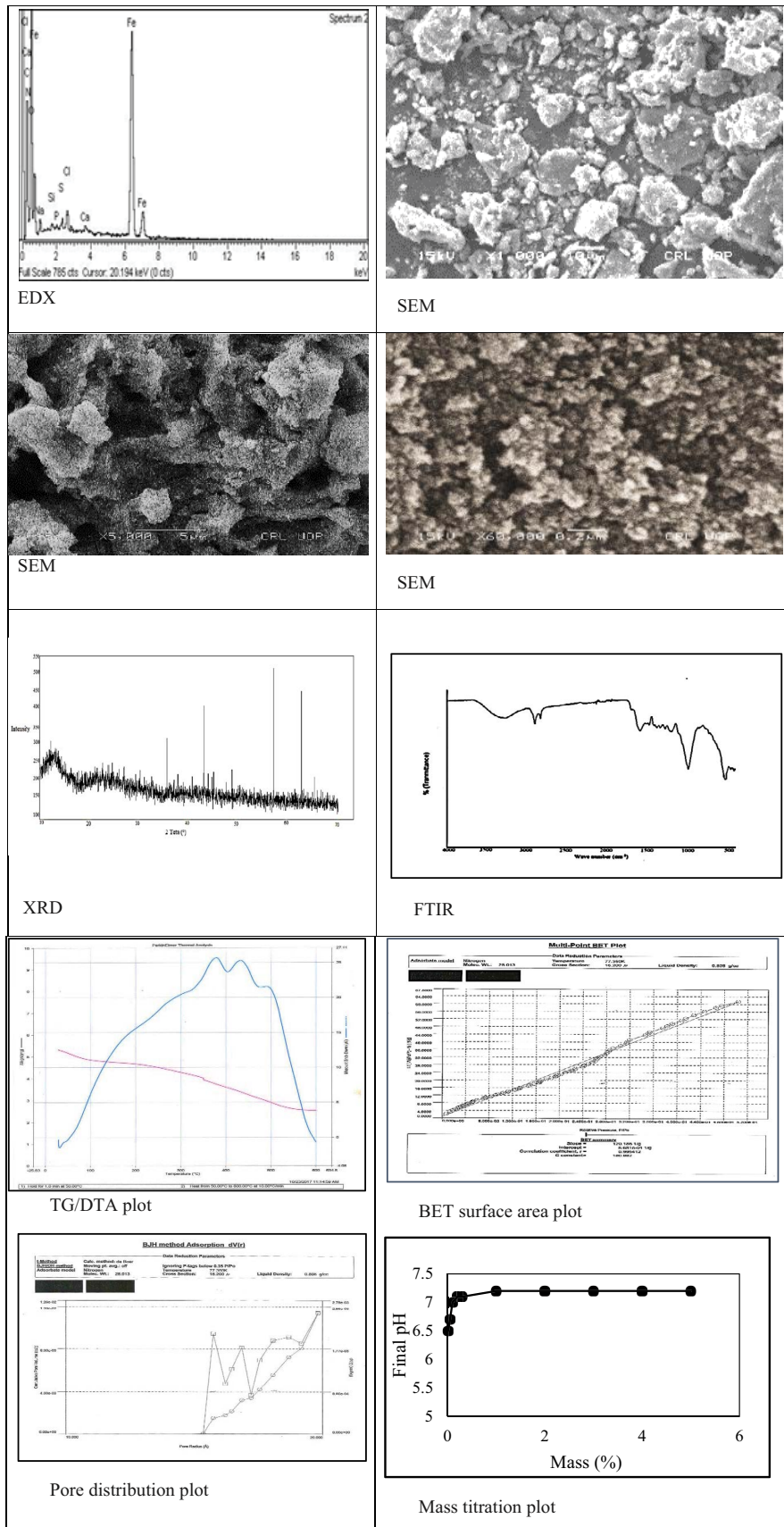


Fig. 2. Instrumental characterization of MCN.

The white spots/patches in the images show the crystallization of the iron oxide in the sample, whereas the black spots/patches represent carbon. The SEM images also show the aggregation of particles due to moisture contents absorbed in the sample. SEM images also explain the cubic crystalline structure of Fe_3O_4 [14,15,17].

XRD method is an important technique used for the structural determination as well as for the measurement of particle size. The XRD spectra of MCN are presented in Fig. 2(e). The spectra show the presence of Fe_3O_4 deposited on the surface of carbon materials. The characteristic diffraction peaks of Fe_3O_4 crystals with cubic crystalline structure in the MCN are evident from the peaks at 2θ values of 30° , 35.7° , 44° , 53° , 57.95° , and 62.5° , which correspond to indices planes of 220, 311, 400, 422, 511, and 400. These values of diffraction peaks correspond to the cubic crystalline structure of magnetite form of iron, which has been previously reported by Zahoor and Maharamanlioglu, Zahoor and Ali Khan, and Mao et al. [15–17]. The other diffraction peaks at 2θ may correspond to other forms of iron such as hematite and maghemite or Fe_3O_4 that may have been changed to $\text{Fe}_3\text{C}/\text{Fe}$ [15,17].

Fig. 2(f) shows FTIR spectra of MCN. The spectra of MCN shows characteristic peaks with broad bands between $3,470$ and $3,200\text{ cm}^{-1}$ in the spectrum which may indicate the presence of surface groups such as phenol, carboxylic acids, carboxylic acid derivatives, as well as the presence of physically adsorbed water on the surface of MCN. The two narrow peaks in the region of $3,000$ – $2,800\text{ cm}^{-1}$ correspond to C–H alkanes, peaks at $1,450$ – $1,600\text{ cm}^{-1}$ correspond to C=C aromatic, peaks at $1,300$ – $1,000\text{ cm}^{-1}$ correspond to –OH alcoholic and ether, while the peaks at 575 – 580 cm^{-1} correspond to Fe–O of magnetite and maghemite [15,17,18].

The thermal analysis (TGA/DTA) of the MCN is given in Fig. 2(g). The initial mass of MCN used was 5.315 mg . The figure shows that first mass loss (8%) from 20°C to 100°C took place. The observed loss in mass is due to loss of water of hydration/crystallization in MCN. The second mass loss step (26%) from 130°C to 350°C can be attributed to thermal degradation of cellulosic materials present in MCN results in the formation of carbonaceous residues. The third mass loss (47%) occurs from 400°C to 540°C , which was due to the phase transition from Fe_3O_4 to FeO , because FeO is thermodynamically stable above 570°C [20]. Above this temperature no further loss in mass of MCN occurs. The final residue was a mixture of ash and carbon. The DTA curve shows three endothermic peaks in the temperature range of 30°C – 490°C .

The surface area analysis of the MCN is shown in Fig. 2(h) while pores distribution graph is given in Fig. 2(i). The surface area, total pore volume, and average pore diameter of the prepared MCN were $39\text{ m}^2/\text{g}$, $0.2\text{ cm}^3/\text{g}$, and 1.975 nm , respectively.

The $\text{pH}_{(\text{pzc})}$ of MCN was also determined using mass titration method and was found to be 7.2 (Fig. 2(j)).

3.2. Adsorption isotherms

The adsorption of CIP from aqueous solutions onto MCN was studied and adsorption isotherm is given in Fig. 3(a). In order to quantitatively describe the adsorption of

CIP by MCN, Langmuir, Freundlich, and Temkin equations were used. The Langmuir adsorption model [21] is based on the assumption that maximum adsorption corresponds to a saturated monolayer of solute molecules formation on the adsorbent surface, with no lateral interaction between the adsorbed molecules.

The linear form of the Langmuir isotherm is given by the following equation:

$$\frac{C_e}{q_e} = \frac{1}{K_L q_m} + \frac{C_e}{q_m} \quad (5)$$

In Eq. (5) q_e is the amount adsorbed (mg/g), C_e is the equilibrium concentration of the adsorbate (mg/L), q_m (mg/g) and K_L (L/mg) are Langmuir constants related to maximum adsorption capacity and energy of adsorption, respectively. The plot of specific adsorption (C_e/q_e) against equilibrium concentration (C_e) shows that adsorption obeys the Langmuir model (Fig. 3(b)). The Langmuir constants q_m and K_L were calculated from the slope and intercept of the plots, and are given in Table 5.

The Freundlich isotherm [22] is an empirical equation employed to explain heterogeneous systems. The logarithmic form of the Freundlich model is given by the following equation:

$$\ln q_e = \ln k + \ln \frac{C_e}{n} \quad (6)$$

In Eq. (6) C_e is the equilibrium concentration (mg/L), q_e is the amount adsorbed (mg/g), k and n are Freundlich constants related to the adsorption capacity and adsorption intensity, respectively. The Freundlich constants, k and n for the MCN, were calculated from the slope and intercept of the plot shown in Fig. 3(c) and are given in Table 5.

The linear form of Temkin isotherm is applied in the following form [23]:

$$C_q = \beta \ln \alpha + \beta \ln C_e \quad (7)$$

where $\beta = RT/b$, T is an absolute temperature in Kelvin (K), R is a general gas constant and its value is 8.314 J/mol/K , while b is related to the heat of adsorption. A straight line is obtained by plotting C_q (where C_q is the amount adsorbed in mg/g) against $\ln C_e$ (equilibrium concentration in mg/L) with slope β and intercept $\beta \ln \alpha$. Different values of Temkin isotherm are calculated from the slope and intercept of Fig. 3(d) and are given in Table 5.

The best fit was obtained with the Langmuir model. The correlation R^2 value for Langmuir model is higher than that of the Freundlich and Temkin models.

3.3. Adsorption kinetics

In wastewater treatment, the contact time required to reach equilibrium is an important factor. Adsorption kinetic studies give us one of the important methodology for explaining the efficiency of an adsorption process and to estimate the time necessary for the adsorbent to reach to equilibrium. The kinetics of CIP adsorption on MCN were

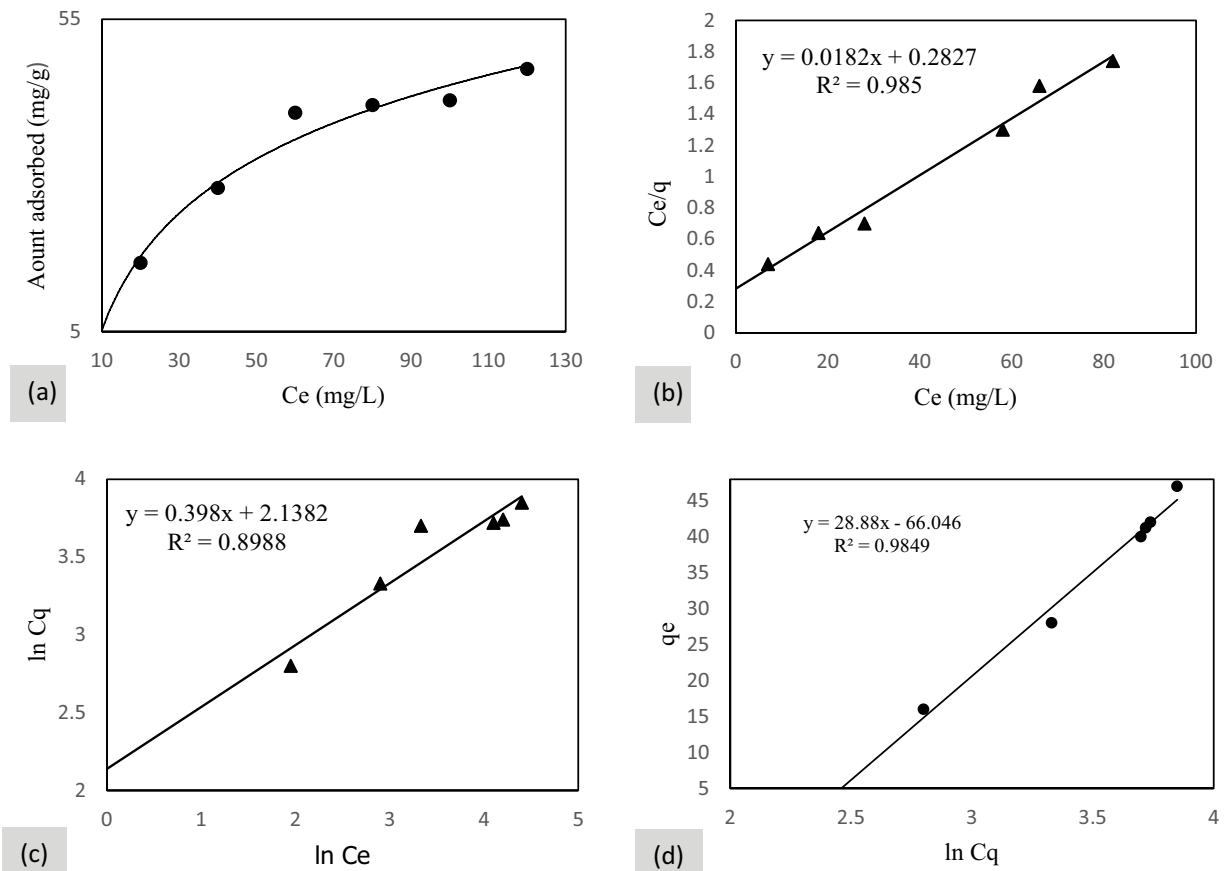


Fig. 3. Adsorption isotherms and effect of concentration on adsorption: (a) effect of concentration on adsorption of MCN, (b) Langmuir plot of CIP adsorption on MCN, (c) Freundlich plot of CIP adsorption on MCN, and (d) Temkin plot of CIP adsorption on MCN.

Table 5
Isotherm parameters for adsorption of CIP onto MCN

Langmuir isotherm	
q_m (mg/g)	55.00
K_L (L/mg)	0.065
R^2	0.99
Freundlich isotherm	
K (mg/g)	137.4
$1/n$	0.34
R^2	0.9
Temkin isotherm	
β	25.88
α	5×10^{-3}
b	84.4
R^2	0.98

investigated for 40 and 80 mg/L initial CIP concentrations. Fig. 4(a) shows the adsorption rate of CIP onto MCN was higher in initial half an hour, the higher rate of adsorption is due to the availability of numerous pores available on MCN surface. When these sites are occupied the rate of adsorption

decreases gradually [19] and finally reached equilibrium. Several kinetic models are used to evaluate the values of the kinetic experiments. Among them, the Lagergren first-order, pseudo-second-order, and intraparticle diffusion models are often successfully used to describe the removal of pollutants from aqueous solution by adsorbents. The mathematical forms of these models are given as follows:

$$\ln(q_e - q_t) = \ln q_e - K_1 t \quad (8)$$

$$\frac{t}{q_t} = \frac{1}{K_2} + \frac{t}{q_e} \quad (9)$$

$$q_t = K_{diff} t^{1/2} + C \quad (10)$$

In Eq. (8) q_t (mg/g) is the amount adsorbed at time t , while q_e (mg/g) is the amount adsorbed at equilibrium time, K_1 (min^{-1}) is the rate constant of pseudo-first-order kinetics. The values of q and K_1 (min^{-1}) were calculated from the slope and intercept of the plot obtained from plotting $\ln(q_e - q_t)$ versus t in Fig. 4(b) and are given in Table 6.

In Eq. (9) K_2 (g/mg/min) is the rate constant of adsorption for pseudo-second-order kinetics, q_e (mg/g) is the amount of CIP adsorbed at equilibrium, while q_t is the amount of CIP

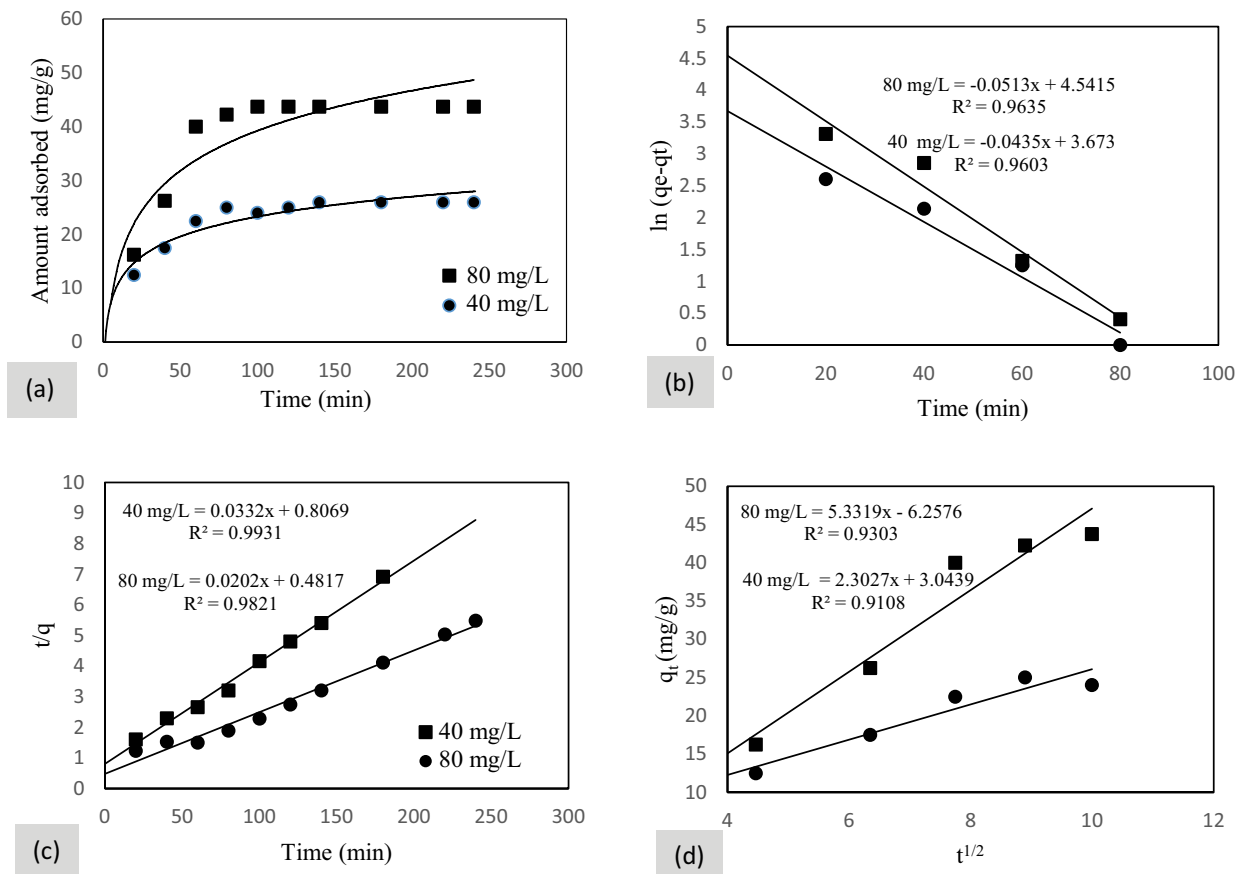


Fig. 4. Adsorption kinetics: (a) Adsorption kinetics plot of CIP adsorption on MCN, (b) pseudo-first-order kinetics plot of CIP adsorption on MCN, (c) pseudo-second-order kinetics plot of CIP adsorption on MCN, and (d) intraparticle diffusion plot of CIP adsorption on MCN.

Table 6
Adsorption kinetics parameters for adsorption of CIP onto MCN

Concentration (mg/L)	Rate constant	Correlation coefficient
Pseudo-second order	K_2 (g/mg/min)	R^2
40	0.0167	0.993
80	0.0101	0.982
Pseudo-first order	K_1 (min^{-1})	R^2
40	0.0435	0.96
80	0.0513	0.96
Intraparticle diffusion model	K_{diff}	C
40	2.3	3.05
80	5.3	6.25

adsorbed at time t . The values of K_2 and q_e were calculated from the slope and intercept of the plot by plotting t/q_t against t in Fig. 4(c) and are given in Table 6.

In Eq. (10), q_t (mg/g) is the amount adsorbed at time t , K_{diff} ($\text{mg/g}/\text{min}^{1/2}$) is intraparticle diffusion constant, and C (mg/g) is the concentration. The values of K_{diff} and C are calculated from the slope and intercept of the plot in Fig. 4(d) and are given in Table 6.

The kinetic parameters calculated from various kinetic models are given in Table 6. It is clear from the results that pseudo-second-order kinetic model fits better the kinetics data than pseudo-first-order kinetic model. Generally, the rate constant K_2 decreases for higher concentration due to limited adsorption sites on the surface of adsorbents [24]. Similar trend has been observed with increase in concentration in this study.

Weber's intraparticle diffusion model was used to determine the adsorption mechanism. The plot of q_t versus $t^{1/2}$ for CIP removal on MCN is given in Fig. 4(e). Generally, if the linear part of the curves passes through the origin of the plot, it can be concluded that intraparticle diffusion is not the only rate-controlling process. The plot of intraparticle diffusion model shows an initial curve followed by linear portion. The initial curve of the plot can be explained by the boundary layer effect, while the linearity of plot corresponds to the intraparticle diffusion phenomena [24,25]. The linear portion of the plot don't pass through plot origin showing that intraparticle diffusion phenomenon is not the only rate controlling step for the sorption of CIP on MCN.

3.4. Adsorption thermodynamics

For the determination of adsorption thermodynamics, the adsorption experiments were carried out at 25°C, 40°C, and 60°C. The Van't Hoff equation was used to determine the values ΔH° and ΔS° .

$$\ln k = \frac{\Delta S^\circ}{R} - \frac{\Delta H^\circ}{RT} \quad (11)$$

In Eq. (11) k is a constant, ΔS° is change in entropy, ΔH° is change in enthalpy, T is temperature in kelvin, and R is a general gas constant. The value of k is determined from the amount of CIP adsorbed and equilibrium concentration. The Van't Hoff plot Fig. 5(a) is obtained by plotting $\ln k$ versus $1/T$ with slope $-\Delta H^\circ/R$ and intercept $\Delta S^\circ/R$. The values of ΔH° and ΔS° were found to be -20 and 82 kJ/mol, respectively.

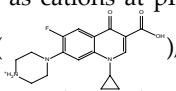
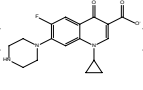
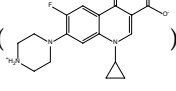
The values of standard free energy ΔG° were calculated using the following equation:

$$\Delta G^\circ = \Delta H^\circ - T\Delta S^\circ \quad (12)$$

The values calculated from equation: -23.6 , -25.6 , and -27.3 kJ/mol correspond to 25°C, 40°C, and 60°C, respectively. The negative values of ΔG° at various temperatures specify the spontaneous nature of the process and a high affinity of CIP molecules for MCN. The rise in ΔG° with the increase in temperature shows that the process of adsorption is more favorable at high temperatures.

3.5. Effect of pH on CIP removal

The CIP adsorption on MCN was investigated at initial pH values between 3 and 11. The results are given in Fig. 5(b). From pH 6 to 9, the adsorption capacity of MCN toward CIP increases gradually as the pH value increases. For CIP, the dissociation constants are 6.1 for $-\text{COOH}$ group ($\text{p}K_{a1}$) and 8.7 for the basic N-moiety ($\text{p}K_{a2}$) [17]. Thus, CIP molecules have three chemically distinct groups and exist as cations at $\text{pH} < 6.1$

due to protonation of amine group (, while at $\text{pH} > 8.7$ CIP molecules exists as anion due to deprotonation of carboxyl group (). Whereas at pH range of 6.1–8.7 CIP molecules exist as zwitterion ().

At pH less than 6 and greater than 9, the adsorption capacities were lower as compared with pH 6–9. This is mainly because the pH value of the solution affects the surface charge of the MCN and the form of antibiotics in the solution [17]. At low pH, the surface of MCN is positively charged due to the protonation reaction. With increasing pH, the surface of MCN becomes negatively charged due to the deprotonation reaction. In addition, the pH value affects the ionization degree of the CIP molecules. At pH range from 6 to 9 the CIP molecules and surface of MCN are oppositely charged, due to which electrostatic forces of attractions are pronounced, leading to higher removal of CIP molecules. The other reason for the removal of CIP molecules is π - π interaction between CIP molecules and MCN. It is clear from molecular structure of CIP molecule that CIP molecule has a benzene ring and two heterocyclic substituents. The presence of F atom on the benzene ring is a strong electron withdrawing group and behaves as π -electron acceptor. The presence of electron donating group on the surface of MCN results in π - π electron donor-accepter interaction leading to high sorption of CIP molecules on MCN surface [17]. Another reason for the removal of CIP molecules may be the formation of H-bond between N-containing groups of CIP molecules with $-\text{OH}$ group of MCN [17].

3.6. Effect of adsorbent dosage on CIP removal

The effect of adsorbent dosage, that is, from 0.01 to 0.06 g at initial CIP concentration of 30 mg/L was determined at 298 K and pH 7. The results in Fig. 5(c) show that the CIP removal increases rapidly with increase in adsorbent dosage that is, from 0.01 to 0.04 g. The increase in CIP removal can be attributed to increase in number of adsorption sites. Onward increase in adsorbent dosage has little effect on adsorption of CIP so, 0.04 g of the MCN dose was selected as optimum dosage and was used in subsequent experiments.

3.7. Effect of HA on CIP removal

HA is common component of aqueous environment and often coexists with antibiotics in wastewater reservoirs. HA molecules contain carboxyl group ($-\text{COOH}$), phenolic ($-\text{OH}$), and many other functional groups, which can interfere with the interactions between CIP and MCN. Therefore, it is of great significance to study the effect of HA on the adsorption process of CIP on prepared adsorbent. In order to study the interference of HA in the adsorption of CIP on MCN different concentrations of HA (0–80 mg/L) were added to mixture (Fig. 5(d)). The figure shows that lower concentration of HA have a minor effect on the % removal of CIP. While the adsorption capacity decreases with increasing HA concentration. This mainly occurs because at low concentration, HA is adsorbed on the surface of MCN by hydrogen bonding, electrostatic attraction, and π - π conjugation, and the groups on the HA molecules can integrate with the CIP molecules. This is the same as increasing the number of adsorption sites on the MCN surface. When the added HA concentration exceeds a certain amount, the amount of free-moving HA molecules in the solution increases [17,26], which competes with the MCN to adsorb CIP ions from the solution, leading to a decrease in the adsorption capacity of MCN.

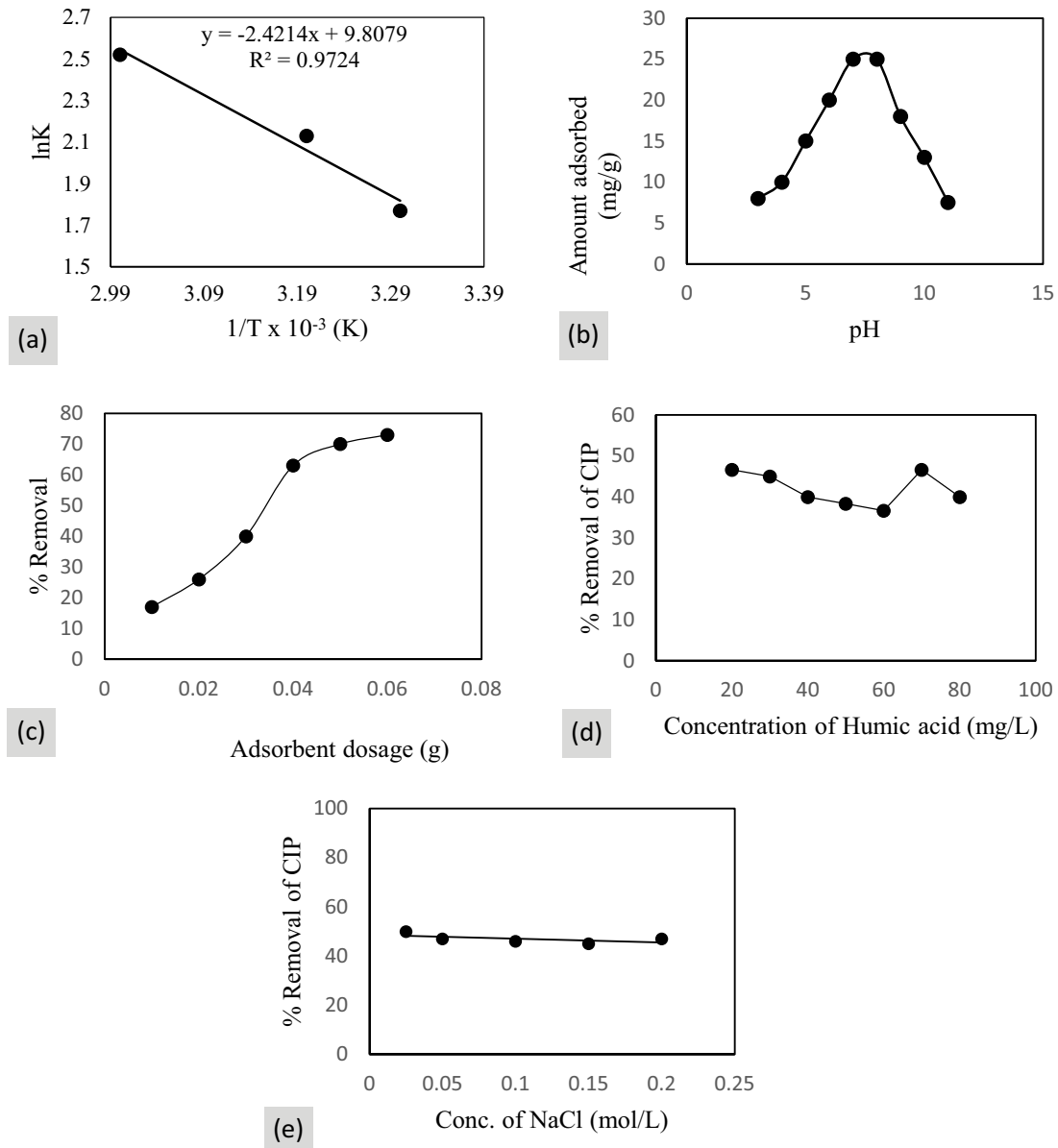


Fig. 5. Effect of various physicochemical parameters on adsorption of CIP on MCN: (a) Van't Hoff plot of CIP adsorption on MCN, (b) pH plot of CIP adsorption on MCN, (c) adsorbent dosage plot of CIP adsorption on MCN, (d) effect of HA plot on CIP adsorption on MCN, and (e) effect of NaCl plot on CIP adsorption on MCN.

3.8. Effect of ionic strength on CIP removal

For the determination of the effect of ionic strength, NaCl was used as ionic substance. The results of effect of ionic strength are given in Fig. 5(e). The results obtained show that ionic strength has little effect on CIP adsorption on MCN. As the concentration of NaCl increases both substances compete for the surface pores on MCN but have a little effect on the adsorption of CIP from aqueous solution in spite of the fact that increase in concentration of NaCl weakens the interaction of CIP particles with MCN [17,26]. The possible reason may be that the Na^+ and Cl^- ions are very small in size that

penetrate inside to internal porous structure of adsorbent leaving the outside pores available for CIP.

3.9. Comparison with other adsorbents

Table 7 shows the adsorption capabilities of various sorbents for the removal of CIP molecules from aqueous media [27–30]. From all these results it is obvious that MCN made from biomass precursors of pineapple have quite satisfactory sorption capability and can easily be removed from solution using external magnet.

3.10. Retention of selected antibiotic by membranes and adsorption/membrane hybrid processes

First the antibiotic solutions were passed through all the three selected membrane systems. The percent retention of CIP for each membrane was calculated. The MWCO of the UF membrane was larger as compared with molecular

Table 7
Comparison of maximum monolayer sorption capacity of CIP with various adsorbents

Adsorbent	Maximum monolayer sorption capacity (mg/g)	Reference
MCN	55	This work
Graphene oxide	39.06	[27]
Modified coal fly ash	1.55	[28]
Aluminum hydroxide	13.6	[29]
Kaolinite	3.26	[30]

weight of CIP [11,13]. Therefore lower percent retention was observed with naked UF membrane as well as MCN/UF processes (Fig. 6(a)).

Definitely high percent retention (almost 100%) was expected from NF and RO system as the MWCO was very small as compared with molecular weight of the selected antibiotic. About 96% retention was observed with NF membrane system (Fig. 6(b)), while 100% retention was observed with RO system (Fig. 6(c)). When the membranes were used in hybrid manner with MCN, the RO was again 100% efficient. The NF percent retention went high up to 100%, while improvement in UF percent retention was also observed but still was not 100% which was due to high MWCO of the UF membrane.

3.11. Effect of CIP on permeate flux of membrane

The effect of CIP on permeate flux is given in Figs. 6(p)–(r). It is clear from these figures that there were a decline in permeate flux in the initial stages for double distilled water through all the three selected membranes, which is due to the

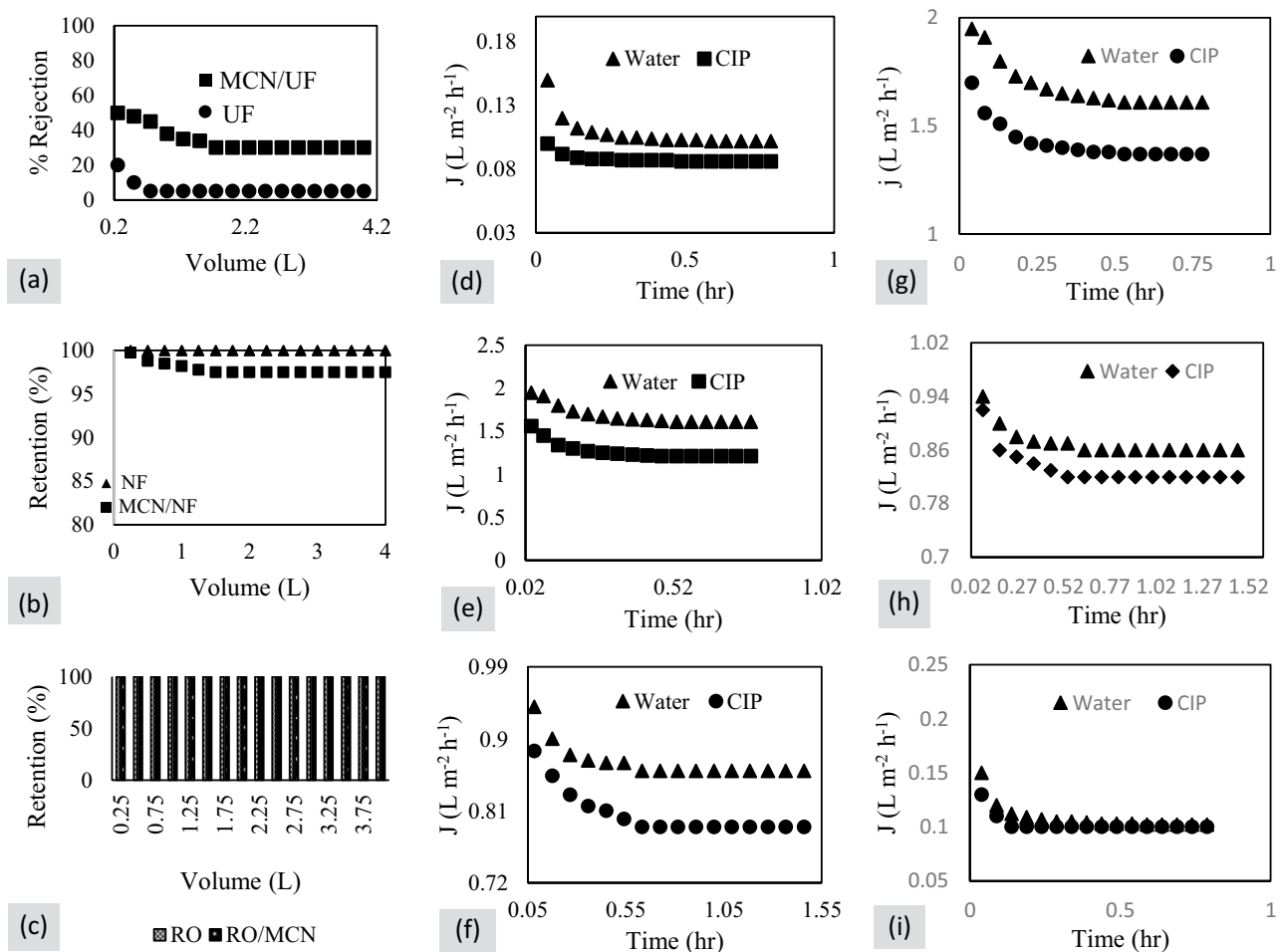


Fig. 6. Effect of MCN on various membrane parameters: (a) percent retention of CIP by UF and MCN/UF, (b) percent retention of CIP by NF and MCN/NF, (c) percent retention of CIP by RO and MCN/RO, (d) effect of CIP on permeate flux of UF, (e) effect of CIP on permeate flux of NF, (f) effect of CIP on permeate flux of RO, (g) improved permeate flux in MCN/UF hybrid membrane, (h) improved permeate flux in MCN/NF hybrid membrane, and (i) improved permeate flux in MCN/RO hybrid membrane.

interaction of the ions present in distilled water and may also due to the intrinsic membrane resistance. In double distilled water usually H^+ and OH^- ions are present, which is clear from the conductance of distilled water (6.3×10^{-5} S/m) [11,13]. The permeate flux then reaches to a steady state and is no longer affected within experimental time and condition. The molecular weight of CIP is smaller than MWCO of UF membrane. CIP molecules are expected to pass freely from UF membrane and the permeate concentration should be equal to that of the bulk concentration (C_b) without addition of MCN in hybrid manner. Apart from low retention, flux reduction was observed. For MCN/UF (Fig. 6(x)) improved permeate flux was observed for the CIP molecules under study than UF membrane alone (Fig. 6(p)). In case of NF and RO membranes the molecular weight of selected antibiotic is larger than MWCO of the membranes, therefore the molecules of CIP were almost 100% retained which consequently affects the permeate flux. The effect of antibiotic on permeate fluxes of NF (Fig. 6(q)) and RO (Fig. 6(r)) was more pronounced. When these membranes were used in hybrid manner with MCN reactor, quite improved fluxes were observed for both NF/MCN (Fig. 6(y)) and RO/MCN (Fig. 6(z)) hybrid processes.

3.12. Backwash time of membrane

After each 50 min cycle backwashing process of membranes were applied with distilled water. The backwashing time taken was much less for MCN prepared from biomass precursors of pineapple because MCN was completely removed from the slurry by application of magnet. This was due to complete removal of MCN, which was removed from solution through the application of magnet. No blackening of the pipes and flowmeter of the membrane system was observed by application of MCN. Thus MCN is useful in membrane system and inexpensive from an economical point of view because it reduces the backwash time of membrane system. Also it has been prepared from low cost biomass precursors.

3.13. Desorption experiments

Regeneration of adsorbents is a key process in practical applications. During regeneration experiments of MCN a

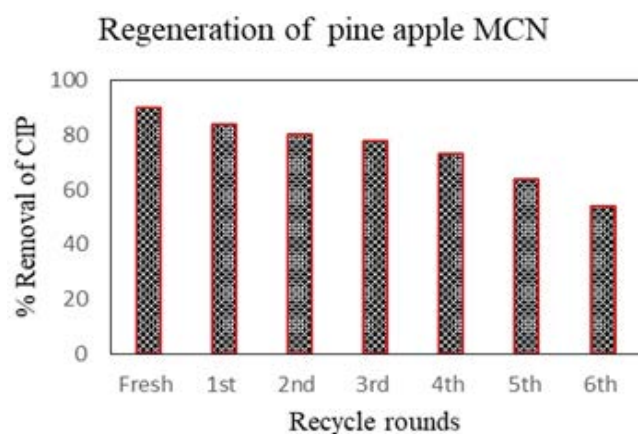


Fig. 7. Regeneration of MCN.

mixture of 20 mL of NaOH solution, 100 mL methanol, and distilled water were used [26]. Fig. 7 shows that adsorption capacity of MCN decreases from 90% to 54% after six rounds of recycling. The decrease in adsorption capacity of regenerated MCN may be due to decrease in specific surface area of MCN and blockage of MCN pores by CIP molecules. As shown in Fig. 7, the adsorption amount of CIP on MCN decreased by 35% after six cycles of adsorption–desorption processes compared with the first adsorption. It is shown that MCN has excellent stability and regeneration properties, and it has an excellent potential as a sorbent for the removal of antibiotics from aqueous media.

4. Conclusion

In this study MCN was prepared from pineapple waste biomass. The novel adsorbent was tested for the removal of CIP from water. Various kinetics and isotherm models were used to describe the experimental data. The kinetic data fits well to pseudo-second-order kinetics model, while adsorption isotherm data fitted well to Langmuir isotherm model rather than Freundlich and Temkin models. ΔS° value was positive, while that of ΔG° and ΔH° were negative. At higher temperature (60°C) the value of ΔG° was high as compared with that at 30°C, which shows that adsorption process is favorable at high temperature. In hybrid membrane processes improvement in permeate fluxes was observed. The MCN can be reused which was evident from its regeneration studies. The retention of CIP by UF membrane was improved and also permeate flux for the hybrid process was little affected. In case of NF membrane improvement in retention time and permeate flux was observed. RO membrane definitely has 100% but the adverse effects of CIP on permeate flux were observable. Improved flux was observed for MCN/RO hybrid process. It was concluded that the MCN can be used as efficient adsorbent for the removal of CIP both in adsorption process alone and in hybrid manner with membrane.

References

- [1] V. Homem, L. Santos, Degradation and removal methods of antibiotics from aqueous matrices, *J. Environ. Manage.*, 92 (2011) 2304–2347.
- [2] O.A. Arikian, W. Mulbry, D. Ingram, Minimally managed composting of beef manure at the pilot scale: effect of manure pile construction on pile temperature profiles and on the fate of ox tetracycline and chlortetracycline, *Bioresour. Technol.*, 100 (2009) 4447–4453.
- [3] M. Nelson, A. Dinardo, J. Hochberg, G. Armelagos, Brief communication: Mass spectroscopic characterization of tetracycline in the skeletal remains of an ancient population from Sudanese Nubia 350–550 CE. *Am. J. Phys. Anthropol.*, 143 (2010) 151–154.
- [4] C. Bouki, D. Venieri, E. Diamadopoulos, Detection and fate of antibiotic resistant bacteria in wastewater treatment plants, *Ecotoxicol. Environ. Saf.*, 91 (2013) 1–9.
- [5] X.V. Doorslaer, J. Dewulf, H.V. Langenhove, Fluoroquinolone antibiotics: an emerging class of environmental micro pollutants, *Sci. Total. Environ.*, 500–501 (2014) 250–269.
- [6] L. Rizzo, C. Manaia, C. Merlin, Urban wastewater treatment plants as hotspots for antibiotic resistant bacteria and genes spread into the environment, *Sci. Total. Environ.*, 447 (2013) 345–360.
- [7] B. Sarkara, N. Venkateswralub, R.N. Raob, C. Bhattacharjee, V. Kalea, Treatment of pesticide contaminated surface water

- for production of potable water by a coagulation–adsorption–nanofiltration approach, *Desalination*, 212 (2007) 129–140.
- [8] A.B. Koltuniewicz, E. Drioli, Membranes in clean technologies, *Membranes*, 31 (2008) 3–11.
- [9] K.V. Plakas, A.J. Karabelas, Removal of pesticides from water by NF and RO membranes—a review, *Desalination*, 287 (2012) 255–265.
- [10] G. Qiu, Y. Song, P. Zeng, L. Duan, S. Xiao, Characterization of bacterial communities in hybrid up flow anaerobic sludge blanket (UASB)–membrane bioreactor (MBR) process for berberine antibiotic wastewater treatment, *Bioresour. Technol.*, 142 (2013) 52–62.
- [11] M. Zahoor, Separation of surfactants from water by granular activated carbon/ultrafiltration hybrid process, *Desal. Wat. Treat.*, 57 (2016) 1988–1994.
- [12] R.W. Holloway, J. Regnery, L.D. Nghiem, T.Y. Cath, Removal of trace organic chemicals and performance of a novel hybrid ultrafiltration-osmotic membrane bioreactor, *Environ. Sci. Technol.*, 48 (2014) 10859–10868.
- [13] M. Zahoor, Effect of granular activated carbon on percent retention of humic acid and permeate flux in GAC/UF membrane process, *Desal. Wat. Treat.*, 57 (2016) 23661–23665.
- [14] M. Zahoor, F.A. Khan, Aflatoxin B1 detoxification by magnetic carbon nanostructure prepared from maize straw, *Desal. Wat. Treat.*, 57 (2015) 11893–11903.
- [15] M. Zahoor, M. Mahramanlioglu, Adsorption of Imidacloprid on powdered activated carbon and magnetic activated carbon, *Chem. Biochem. Eng. Q.*, 25 (2011) 55–63.
- [16] M. Mahramanlioglu, M. Zahoor, M. Kizilcikli, Removal of phenol red by activated and magnetic activated carbon, *Fresenius Environ. Bull.*, 19 (2010) 911–918.
- [17] H. Mao, S. Wang, J.Y. Lin, Z. Wang, J. Ren, Modification of magnetic carbon composites for CIP adsorption, *J. Environ. Sci.*, 49 (2016) 179–188.
- [18] J. Zheng, Z. Liu, X.S. Zhao, M. Liu, X. Liu, W. Chu, One step solvothermal synthesis of Fe₃O₄/C core shell nanoparticles with tunable sizes, *Nanotechnology*, 23 (2012) 165601–165608.
- [19] X. Bao, Z. Qiang, J.H. Chang, W. Ben, J. Qu, Synthesis of carbon coated magnetic nanoparticles (Fe₃O₄/C) and its applications for sulfonamide antibiotics removal from water, *J. Environ. Sci.*, 26 (2014) 962–969.
- [20] M. Mahdavi, M.B. Ahmad, M.J. Haron, F. Namvar, B. Nadi, M.Z.A. Rahman, J. Amin, Synthesis, surface modification and characterization of biocompatible magnetic iron oxide nanoparticles for biomedical applications, *Molecules*, 18 (2013) 7534–7547.
- [21] Langmuir, The adsorption of gases on plane surfaces of glass, mica and platinum, *J. Am. Chem. Soc.*, 40 (1918) 1361–1403.
- [22] H. Freundlich, Über die adsorption in losungen (adsorption in solution), *Z. Phys. Chem.*, 57 (1906) 384–470.
- [23] C. Perk, J.B. Joo, J. Yi, Adsorption of acid dyes using polyelectrolyte impregnated mesoporous silica, *Korean J. Chem. Eng.*, 22 (2005) 276–280.
- [24] J.N. Genc, E.C. Dogan, Adsorption kinetics of the antibiotic Ciprofloxacin on bentonite, activated carbon, zeolite and pumice, *Desal. Wat. Treat.*, 53 (2015) 785–793.
- [25] W. Plazinski, W. Rudzinski, A. Plazinska, Theoretical models of sorption kinetics including a surface reaction mechanism: a review, *Adv. Colloid Interface Sci.*, 152 (2009) 2–13.
- [26] Y. Gao, Y. Li, L. Zhang, H. Huang, J. Hu, S.M. Shah, X.G. Su, Adsorption and removal of tetracycline antibiotics from aqueous solution by graphene oxide, *J. Colloid Interface Sci.*, 368 (2012) 540–546.
- [27] S. Wu, X. Zhao, Y. Li, C. Zhao, Q. Du, J. Sun, Y. Wang, X. Peng, Y. Xia, Z. Wang, Adsorption of ciprofloxacin onto bio composite fibers of graphene oxide/calcium alginate, *Chem. Eng. J.*, 230 (2013) 389–395.
- [28] C.L. Zhang, G.L. Qiao, F. Zhao, Y. Wang, Thermodynamic and kinetic parameters of ciprofloxacin adsorption onto modified coal fly ash from aqueous solution, *J. Mol. Liq.*, 163 (2011) 53–56.
- [29] C. Gu, K. Karthikeyan, Sorption of the antimicrobial ciprofloxacin to aluminum and iron hydrous oxides, *Environ. Sci. Technol.*, 39 (2005) 9166–9173.
- [30] Z. Li, H. Hong, L. Liao, C.J. Ackley, L.A. Schulz, R.A. MacDonald, A.L. Mihelich, S.M. Emard, A mechanistic study of ciprofloxacin removal by kaolinite, *Colloids Surf., B*, 88 (2011) 339–344.